厚生労働科学研究費補助金（障害者対策総合研究事業（神経・筋疾患分野））
分担研究報告書

非典型レット症候群の原因遺伝子 *CDKL5* の遺伝子変異による病態機序の解析

研究分担者　田中輝幸　東京大学大学院医学系研究科発達医科学教室・准教授

研究要旨
非典型レット症候群の原因遺伝子 *CDKL5* の遺伝子変異による病態機序の解明を目的として、独自に作製した *Cdk15* ノックアウト（KO）マウスの神経科学的解析を行った。その結果 *Cdk15* KO マウスにおいて、海馬神経細胞樹状突起スパインの形態・密度異常、易痙攣性、シナプスグルタミン酸受容体機能・蛋白質の異常を同定し、グルタミン酸受容体阻害薬による興奮性アミノ酸誘発性けいれんのレスキューに成功した。以上の成果から、*CDKL5* 変異に伴う病態が興奮性シナプス機能異常である事が示され、グルタミン酸受容体作動薬による治療の基盤が見出された。

A．研究目的

Cyclin-dependent kinase-like 5 (CDKL5) 遺伝子は早期発症てんかんを伴う非典型レット症候群の原因遺伝子である。しかしその遺伝子変異による病態機序及び根本的治療法は未解明である。私はこれらの問題解決を目指し、*Cdk15* ノックアウト(KO)マウスを作製し、神経科学的解析を行った。本研究の目的は、*Cdk15* KO マウスのてんかん、記憶障害、情動異常等の発達障害のメカニズムの解明である。

B．研究方法

・ *Cdk15* KO マウスの表現型解析
(1) 神経細胞樹状突起及びスパインの解析
(2) 薬物投与による易けいれん性解析
(3) 海馬スライスの電気生理学的解析
(4) 海馬・大脳皮質の興奮性シナプスの機能、微細構造、蛋白質解析
(5) グルタミン酸受容体阻害薬による興奮性アミノ酸誘発性けいれんのレスキュー

C．研究結果

・ *Cdk15* KO マウス異常表現型解析
Cdk15 KO マウスにおいて、海馬 CA1 錐体ニューロンの樹状突起スパインの形態、サブクラス、及び密度に異常が認められた。KO マウスに対する興奮性アミノ酸投与によって、過剰な強いけいれんが誘発された。海馬スライスの電気生理学的解析により、KO マウスにおける長期増強（LTP）の異常、脱分極の異常等を同定した。生化学的手法及び免疫電子顕微鏡を用いた KO マウスの興奮性シナプス解析により、NMDA 型グルタミン酸受容体サブユニットの構成異常及び足場蛋白質の増加を同定した。更に、NMDA 型グルタミン酸受容体の阻害薬投与により、興奮性アミノ酸誘発性けいれんが、野生型と同レベルまで軽減し、致死性のけいれんをレスキューした。

D．考察

Cdk15 KOマウスでは神経細胞樹状突起において未熟なスパインが有意に増加していることが明らかとなった。興奮性アミノ酸に対する過剰興奮、興奮性ニューロンのNMDA型グルタミン酸受容体蛋白質の異常、電気生理学的異常などから、本KOマウスにおけるグルタミン酸シグナリング障害が明らかとなった。
NMDA型グルタミン酸受容体阻害薬による興奮性アミノ酸誘発性けいれんのレスキューの成功は、上記の病態機序に対する分子治療法の開発の基盤となるものである。本研究結果から、*CDKL5*遺伝子変異による発達障害の病態が興奮性シナプス機能異常であることが示され、治療の方策の一つが見出せた。

E．結論

Cdk15 KO マウスの神経科学的解析によって、記憶・学習・情動に極めて重要な働きを担う海馬の神経細胞樹状突起スパインの形態・密度とシナプスグルタミン酸受容体蛋白質の異常、シナプス機能異常が同定され、グルタミン酸受容体阻害薬によって KO マウスの興奮性アミノ酸誘発性けいれんをレスキューする事が出来た。

F．研究発表

1．論文発表

1. 奥田耕助，田中輝幸．難治性てんかんを伴う神経発達障害の原因遺伝子*CDKL5*のシナプス伝達調節機構の解明に向けて．日本薬理学雑誌．2015（in press）．

2．学会発表

1. 田中輝幸．小児の難治性てんかんとCDKL5．第70回東海てんかん集談会．（浜松）(2014.2.1)．
2. 奥田耕助，田中輝幸「難治性てんかんを伴う重度発達障害の原因遺伝子 CDKL5 のシナプス伝達調節機能と情動・記憶における役割」（シンポジウム：X-連鎖知的障害の分子病態解明への挑戦）」 第 87 回日本薬理学会年会（仙台）(2014.3.21)．
3. 田中輝幸，渡邉紀，萩原舞，村上拓冬，小林静香，真鍋俊也，高雄啓三，宮川剛，深谷昌弘，阪上洋行，水口雅，奥田耕助．神経発達障害原因遺

伝子 *CDKL5* の機能解析. 第 37 回日本神経科学大会 Neuro 2014 (2014. 9.13).

G．知的所有権の取得状況
特許取得、実用新案登録　なし

厚生労働科学研究費補助金（障害者対策総合研究事業（神経・筋疾患分野））
分担研究報告書

インプリンティング遺伝子の細胞生物学的解析

研究分担者　堀家慎一　金沢大学学際科学実験センター・准教授
研究協力者　堀家牧子　金沢大学学際科学実験センター・博士研究員

研究要旨
本研究では、レット症候群（RTT）の原因遺伝子であるメチル化 CpG 結合タンパク 2（MeCP2）の Prader-Willi/Angelman 症候群(AS)責任遺伝子座における分子動態を解明する。最近、自閉症やレット症候群患者の脳神経細胞において、15ｑ11-ｑ13 領域のクロマチン動態が適切な神経特異的な遺伝子発現にとって大変重要であることが示された。そこで、15ｑ11-ｑ13 領域のクロマチン動態がどのように制御されているか明らかにし、新たな治療法の開発へ発展させる。

Ａ．研究目的

15ｑ11-ｑ13 領域は、類縁疾患である Angelman 症候群(AS)や Prader-Willi 症候群（PWS）の責任遺伝子座であり、メチル化 CpG 結合タンパク 2（MeCP2）を介したエピゲノム機構によって遺伝子発現が制御されている。最近、レット症候群(RTT)や自閉症患者において 15ｑ11-ｑ13 領域のクロマチン動態の異常が報告され、MeCP2 がエピゲノム機構を介したクロマチン動態の制御に重要な役割を果たしている可能性が示唆された。そこで、この 15ｑ11-ｑ13 領域における MeCP2 の分子動態を解明することで、RTT のみならず AS や PWS、自閉症などの類縁疾患の発症病態の解明へも発展させる。

Ｂ．研究方法

親由来の明らかなヒト 15 番染色体を１本保持したマウス F12 細胞（神経様細胞株）において、15ｑ11-ｑ13 領域のインプリンティングセンター（PWS-IC）がどのように染色体ドメインレベルの遺伝子発現及びクロマチン動態を規定しているか明らかにするため、ヒト染色体工学技術を用いて PWS-IC を欠失させた改変ヒト 15 番染色体を各々構築し、前年度に引き続き qRT-PCR、DNA メチル化解析、DNA-FISH 法、ChIP 法で 15q11-q13 領域のクロマチン動態と遺伝子発現がどのように制御されているか解析する。

（倫理面への配慮）

本研究では、確立された培養細胞を用いた実験であり、遺伝子組み換えにおいては金沢大学遺伝子組換え DNA 安全委員会の承認を得ている。

Ｃ．研究結果

前年度までに、ヒト染色体工学技術を用いて PWS-IC を欠失させた改変母方 15 番染色体および改変父方 15 番染色体の構築に成功した。構築した PWS-IC 欠失染色体で、15ｑ11-ｑ13 領域の遺伝子発現を qRT-PCR 法で解析したところ、父方特異的な MAGEL2 遺伝子の発現低下が認められた。そこで、本年度は DNA-FISH 法により 15ｑ11-ｑ13 領域のクロマチン動態を詳細に解析することで、MAGEL2 遺伝子の発現低下を引き起こしたクロマチン動態を明らかにすることとした。その結果、父方アレル特異的なクロマチン脱凝集は PWS-IC を欠失したにも関わらずクロマチン脱凝集状態を維持していた。一方、PWS-IC 欠失母方染色体では異所的にクロマチン脱凝集が起こっていた。さらに、15 番染色体テリトリーと MAGEL2 遺伝子座の相関関係について解析したところ、発現している MAGEL2 遺伝子座は 15 番染色体テリトリーの外側にループアウトし、発現していない MAGEL2 遺伝子座は 15 番染色体テリトリーの内側にあることが明らかとなった。

Ｄ．考察

15ｑ11-ｑ13 領域は、ゲノム刷り込みを受け、親アレル特異的な遺伝子発現及びクロマチン動態を呈する。PWS-IC 欠失父方染色体において、父方アレル特異的なクロマチン脱凝集が維持されていたことは、父方アレル特異的なクロマチン脱凝集の形成・維持に父性発現を呈する長鎖ノンコーディング RNA、*UBE3A-ATS* の転写が必要ないことを示唆している。逆に、PWS-IC 欠失母方染色体において異所的にクロマチン脱凝集が生じたことから、MeCP2 などのメチル化 CpG を認識する分子が正常母方アレルにおけるコンパクトなクロマチン状態の維持に重要であることが示された。一方、父方 PWS-IC が 1Mb 離れた MAGEL2 遺伝子座の核内配置をコントロールしている事実は大変興味深く、今後 15ｑ11-ｑ13 領域のクロマチン状態の形成・維持に関わる因子を同定すると共に、MeCP2 を介した遺伝子発現制御機構を明らかにする。さらに、RTT の治療のターゲットとなる分子の同定を試みると共に、治療法の開発へ発展させる。

Ｅ．結論

MeCP2 による 15ｑ11-ｑ13 領域の遺伝子発現制御機構を明らかにすることは、RTT の複雑な病態を明らかにする上で極めて重要である。本研究では、MeCP2 などのメチル化 PWS-IC に結合する因子が 15q11-q13 領域のクロマチン脱凝集などの高次クロマチン構造

を介して神経細胞特異的な遺伝子発現を制御していることを見出した。この 15ｑ11-ｑ13 領域の高次クロマチン動態には、MeCP2 などのメチル化 CpG 結合蛋白質が中心的役割を担っていると考えられ、その作用機序の解明は RTT のみならず AS や PWS、自閉症など発症機序の解明につながる可能性が示唆された。

Ｇ．研究発表

１．論文発表

1. Meguro-Horike, M., Horike, S. (2015) MMCT-Mediated Chromosome engineering technique applicable to functional analysis of lncRNA and nuclear dynamics. *Methods Mol Biol*, 1262; 277-289.
2. 目黒牧子，堀家慎一「発達障害の遺伝学から明らかとなる多彩なエピジェネティクスの役割」エピジェネティクスの産業応用，シーエムシー出版，2014 年 4 月

２．学会発表

1. 堀家慎一，Yasui DH, Powell W, LaSalle JM, 目黒一堀家牧子 「PWS-IC is essential for the higher order chromatin organization of 15q11-q13 and the location of a paternally expressed gene within a chromosome 15 territory」高等研カンファレンス Chromatin Decoding，国際高等研究所，京都，2014 年 5 月 12～15 日
2. 堀家慎一，Yasui DH, LaSalle JM, Resnick JL, 目黒牧子「高次クロマチンダイナミクスを制御する PWS-IC の新たな役割」日本生化学会北陸支部 第 32 回大会，富山，2014 年 5 月 24 日
3. 目黒牧子，堀家慎一「クロマチンダイナミクスを制御する PWS/AS インプリンティングセンターの新たな役割」 第 8 回日本エピジェネティクス研究会，伊藤国際学術センター，東京，2014 年 5 月 25～27 日
4. 堀家慎一，Yasui DH, LaSalle JM, Resnick JL, 目黒牧子「高次クロマチンダイナミクスを介した PWS-IC による遺伝子発現制御機構の解析」第 8 回日本エピジェネティクス研究会，伊藤国際学術センター，東京，2014 年 5 月 25～27 日
5. 堀家慎一【招待講演】「核内ダイナミクスと遺伝子発現」名市大エピジェネティクス研究会，ホテル木曽路，南木曽，2014 年 9 月 4～5 日
6. 堀家慎一【招待講演】「発達障害におけるエピジェネティクス研究」第 57 回日本神経化学会大会・第 36 回日本生物学的精神医学会，奈良県文化会館，奈良，2014 年 9 月 29～10 月 1 日
7. 目黒牧子，赤木佐千代，＊堀家慎一「CRISPR/Cas システムを用いたヒト染色体ドメインの大規模欠失によるクロマチンダイナミクスの解析」第 4 回ゲノム編集研究会，広島国際会議場，広島，2014 年 10 月 6～7 日
8. Horike S. MeCP2 is required for chromatin higher-order structure and dynamics at the imprinted 15q11-q13 locus. Epigenomics of Common Diseases, Wellcome Trust Conference Centre, Churchill College, Cambridge, UK 2014 年 10 月 28～31 日
9. 堀家慎一，Yasui DH, LaSalle JM, Resnick JL, 目黒牧子「高次クロマチンダイナミクスを制御する PWS-IC の新たな役割」第 32 回染色体ワークショップ，第 13 回核ダイナミクス研究会，広島，2014 年 12 月 15～17 日
9. S Horike, DH Yasui, W Powell, JM LaSalle, M Meguro-Horike. PWS-IC is essential for the higher order chromatin organization of 15q11-q13 and the location of a paternally expressed gene within a chromosome 15 territory. The 4D Nucleome 2014, Hiroshima, 2014 年 12 月 17～20 日

Ｈ．知的財産権の出願・登録状況

なし

III. 研究成果の刊行に関する一覧表

研究成果の刊行に関する一覧表

書籍

著者氏名	論文タイトル名	書籍全体の編集者名	書　籍　名	出版社名	出版地	出版年	ページ
伊藤雅之，青天目信，高橋悟，原宗嗣，白川哲夫，田村文誉，梶浦一郎，森崎市治郎		青天目信、伊藤雅之	レット症候群診療ガイドブック	大阪大学出版会	大阪	2015	
松石豊次郎	PCD（一次性〈全身性〉カルニチン欠損症）	杉江秀夫	代謝性ミオパチー	診断と治療社	東京	2014	101-104
目黒牧子，堀家慎一	発達障害の遺伝学から明らかとなる多彩なエピジェネティクスの役割		エピジェネティクスの産業応用	シーエムシー出版		2014	
Meguro-Horike M, Horike S.	MMCT-Mediated Chromosome engineering technique applicable to functional analysis of lncRNA and nuclear dynamics.	S. Nakagawa, T. Hirose	Nuclear Bodies and Noncoding RNAs	Springer New York	New York	2015	277-289

雑誌

発表者氏名	論文タイトル名	発表誌名	巻号	ページ	出版年
Ohba C, Nabatame S, Iijima Y, Nishiyama K, Tsurusaki Y, Nakashima M, Miyake N, Tanaka F, Ozono K, Saitsu H, Matsumoto N.	De novo WDR45 mutation in a patient showing clinically Rett syndrome with childhood iron deposition in brain.	J Hum Genet	59(5)	292-5	2014
奥田耕助，田中輝幸	難治性てんかんを伴う神経発達障害の原因遺伝子*CDKL5*のシナプス伝達調節機構の解明に向けて	日本薬理学雑誌			2015 (in press)
Meguro-Horike M, Horike S.	MMCT-Mediated Chromosome engineering technique applicable to functional analysis of lncRNA and nuclear dynamics.	*Methods Mol Biol*	1262	277-289	2015
Kumakura A, Takahashi S, Okajima K, Hata D	A haploinsufficiency of FOXG1 identified in a boy with congenital variant of Rett syndrome.	Brain Dev	36	725-729	2014

Hara M, Nishi Y, Yamashita Y, Hirata R, Takahashi S, Nagamitsu S, Hosoda H, Kangawa K, Kojima M, Matsuishi T	Relation between circulating levels of GH, IGF-1, ghrelin and somatic growth in Rett Syndrome.	Brain Dev	36	794-800	2014
高橋 悟	Rett症候群の病態理解 -病因遺伝子（*MECP2, CDKL5, FOXG1*）変異に関連した臨床的特徴について-	脳と発達	46	117-120	2014
Sato M, Toriumi T, Watanabe N, Watanabe E, Akita D, Mashimo T, Akiyama Y, Isokawa K, Shirakawa T, Honda M.	Characterization of mesenchymal progenitor cells in crown and root pulp from human mesiodentes.	Oral Dis	21	e86-e97	2015
Aono Y, Taguchi H, Saigusa T, Uchida T, Takada K, Takiguchi H, Shirakawa T, Shimizu N, Koshikawa N, Cools AR.	Simultaneous activation of the α1A-, α1B- and α1D-adrenoceptor subtypes in the nucleus accumbens reduces accumbal dopamine efflux in freely moving rats.	Behav Pharmacol	26	73-80	2015
Yamasaki M, Okada R, Takasaki C, Toki S, Fukaya M, Natsume R, Sakimura K, Mishina M, Shirakawa T, Watanabe M.	Opposing role of NMDA receptor GluN2B and GluN2D in somatosensory development and maturation.	J Neurosci	34	11534-11548	2014
Nakamura H, Kato R, Shirakawa T, Koshikawa N, Kobayashi M	Spatiotemporal profiles of dental pulp nociception in rat cerebral cortex: An optical imaging study.	J Comp Neurol			2015 (in press)
Waga C, Asano H, Tsuchiya A, Itoh M, Goto Y, Kohsaka S, Uchino S.	Identification of novel SHANK3 transcript in the developing mouse neocortex.	*J Neurochem*	128	280-293	2014

Ⅳ．研究成果の刊行物・別刷

ELSEVIER

Brain & Development 36 (2014) 725–729

BRAIN & DEVELOPMENT
Official Journal of the Japanese Society of Child Neurology

www.elsevier.com/locate/braindev

Case report

A haploinsufficiency of *FOXG1* identified in a boy with congenital variant of Rett syndrome

Akira Kumakura [a,*], Satoru Takahashi [b], Kazuki Okajima [b], Daisuke Hata [a]

[a] *Department of Pediatrics, Kitano Hospital, The Tazuke Kofukai Medical Institute, Osaka, Japan*
[b] *Department of Pediatrics, Asahikawa Medical University, Asahikawa, Japan*

Received 10 November 2012; received in revised form 1 September 2013; accepted 13 September 2013

Abstract

Background: Forkhead box G1 gene (*FOXG1*) mutations and deletions are associated with a congenital variant of Rett syndrome (RTT). Nucleotide alterations of the coding region of *FOXG1* have never caused dysmorphic features. *Patient:* An 8-year-old boy with the congenital variant of RTT who showed severe psychomotor deterioration, epilepsy, acquired microcephaly, and involuntary movements including jerky movements of the upper limbs and tongue protrusion. He showed dysmorphic features including round face, anteverted nostrils, and tented upper lips. Brain magnetic resonance imaging showed hypoplasia of the frontal lobes and the rostral part of the corpus callosum. The molecular cytogenetic analysis confirmed a *de novo* deletion of 14q12 including *FOXG1* in this patient. *Conclusion:* We identified the smallest deletion of 14q12 involving *FOXG1* among those previously reported. Dysmorphic facial features are a characteristic for the patients with chromosomal deletion including *FOXG1*. In our patient, *C14orf23* is the only transcript other than *FOXG1*. Therefore, *C14orf23* might be responsible for facial dysmorphism.

Keywords: Rett syndrome; Congenital variant; *FOXG1*; *C14orf23*; Dismorphic facial features

1. Introduction

Rett syndrome (RTT), a severe neurodevelopmental disorder with characteristic clinical features including psychomotor deterioration, acquired microcephaly, seizures, and loss of purposeful hand movements, has incidence of 1:10,000 female births. It is the second most common cause of severe mental retardation in females. About 90% of typical RTT cases are attributable to mutations in the methyl-CpG-binding protein 2 gene (*MECP2*) located on the X chromosome. Therefore, the affected patients have been exclusively females [1]. Mutational analyses conducted for RTT patients without *MECP2* abnormalities have revealed mutations in the cyclin-dependent kinase-like 5 gene (*CDKL5*) on Xp22 or mutations in the forkhead box G1 gene (*FOXG1*) on 14q12. *CDKL5* mutations are associated with the early onset seizures variant of RTT in both females and males [2,3]. Both loss of function mutations and microdeletions of *FOXG1* have been identified in patients with the congenital variant of RTT, accounting for 0.6% in patients with RTT [4–9]. The congenital variant of RTT is characterized by brain malformation that is specific to the forebrain, severe psychomotor deterioration, and involuntary movements including tongue protrusion and stereotyped jerky movements of the upper limbs. *FOXG1* is a brain-specific transcriptional factor that is necessary for fetal neurogenesis. Lack of *FOXG1* function suppresses neural stem cell self-renewal and promotes premature cortical neural expansion, engendering

* Corresponding author. Address: Department of Pediatrics, Kitano Hospital, The Tazuke Kofukai Medical Institute, 2-4-20 Ohgimachi, Kita-Ku, Osaka 530-8480, Japan. Tel.: +81 6 6312 8824; fax: +81 6 6312 8867.
E-mail address: a-kumakura@kitano-hp.or.jp (A. Kumakura).

0387-7604/$ - see front matter © 2013 The Japanese Society of Child Neurology. Published by Elsevier B.V. All rights reserved.
http://dx.doi.org/10.1016/j.braindev.2013.09.006

an insufficient quantity of telencephalic neurons [10–12]. This report describes a Japanese boy who showed postnatal developmental deterioration and arrested head growth after 10 months of age. Moreover, he showed irregular jerky movements of the upper limbs. We initially diagnosed him as having dyskinetic or athetotic cerebral palsy. However, according to the diagnostic criteria for classical and variant RTT [13], this patient was regarded as having a congenital variant of RTT. Therefore, we conducted *FOXG1* mutational analysis, which revealed a *de novo* deletion of *FOXG1* at 14q12.

2. Case report

The patient, an 8-year-old boy, was born to non-consanguineous, healthy Japanese parents at 38 weeks gestation after an uneventful pregnancy. His birth weight and length were, respectively, 2680 g (−0.78 SD) and 49.0 cm (−0.17 SD). He had normal occipito–frontal circumference (OFC) of 32.0 cm (−0.86 SD) with no auxological abnormality. He showed no asphyxia or jaundice. He had no siblings and no family history of neuromuscular diseases, metabolic disorders, dysmorphic syndrome, or other developmental disorders. He had developed with no complications during the neonatal period. However, he showed developmental delay and deterioration after 3 months of age. His motor skills had progressed to rolling over. Subsequently, his head control deteriorated and he became less able to roll over, being bedridden. He showed severe mental retardation with no explosive language, but with deficient social reciprocal communication including eye contact and eye

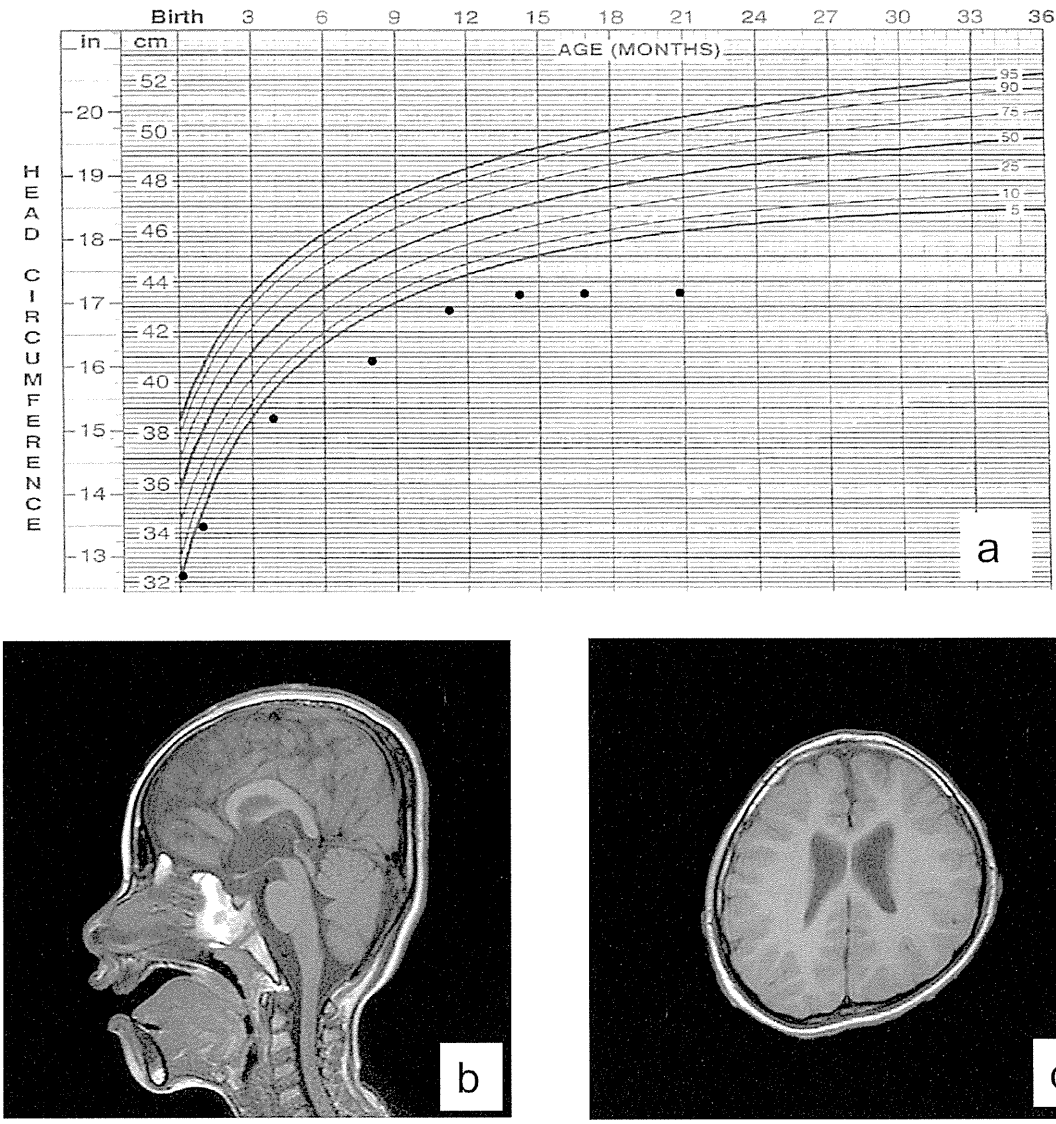

Fig. 1. (a) Growth curve of occipito-frontal circumference shows postnatal microcephaly became more evident between 4 and 8 months of age. (b and c) Brain magnetic resonance imaging (MRI) shows hypoplasia of the rostral part of the corpus callosum ((b) TR/TE = 529.283/13.000) and frontal lobes ((c) TR/TE = 505.224/13.000).

gaze. His sleep pattern did not acquire circadian rhythm. He needed no enteral tube feeding. Postnatal microcephaly became more evident at 4–8 months of age (Fig. 1a). In addition to acquired microcephaly, he had dysmorphisms including a round face, anteverted nostrils, and tented upper lips. Physical examination revealed severe truncal hypotonia. He demonstrated dyskinesic involuntary movements: peculiar jerky movements of the upper limbs pushed in different directions and tongue protrusion. He showed no stereotypic hand washing or hand mouthing, as patients with RTT typically do. Ophthalmological and audiological examinations yielded normal results. Chromosomal analysis revealed normal karyotype, 46, XY. Extensive metabolic investigations including serum amino-acid quantification, serum acylcarnitine profile quantification, and urine organic acid quantification revealed no abnormality.

At three years of age, he experienced unprovoked seizures: nocturnal tonic seizures and sometimes hypermotor seizures. Interictal electroencephalography (EEG) revealed sharp waves over the bilateral frontopolar areas. Therefore, we diagnosed him as having symptomatic focal epilepsy. Brain magnetic resonance imaging (MRI) revealed hypoplasia of the frontal lobes and the rostral part of the corpus callosum (Fig. 1b and c). Antiepileptic drugs including zonisamide, phenytoin, and phenobarbital controlled his epileptic seizures well. From six years of age, atypical absence and tonic seizures appeared. Interictal EEG showed high-amplitude slow activity and diffuse slow spike and wave complex predominantly over the frontal areas. These seizures were treated with valproate, topiramate, and lamotrigine, which produced some improvement in seizure frequency. These clinical and radiological features are compatible with those of the congenital variant of RTT.

3. Genetic analysis

After obtaining written informed consent from his parents, genomic DNA was extracted from the peripheral blood leukocytes of the patient and his parents and was used for mutation screening. The compatible primers for polymerase chain reaction (PCR) were used to obtain DNA fragments spanning the entire *FOXG1* coding region [4]. Mutation screenings were performed by direct sequencing of the exon1-derived PCR products. Direct sequencing of the entire *FOXG1* coding region yielded a normal result. Screening of the patient's

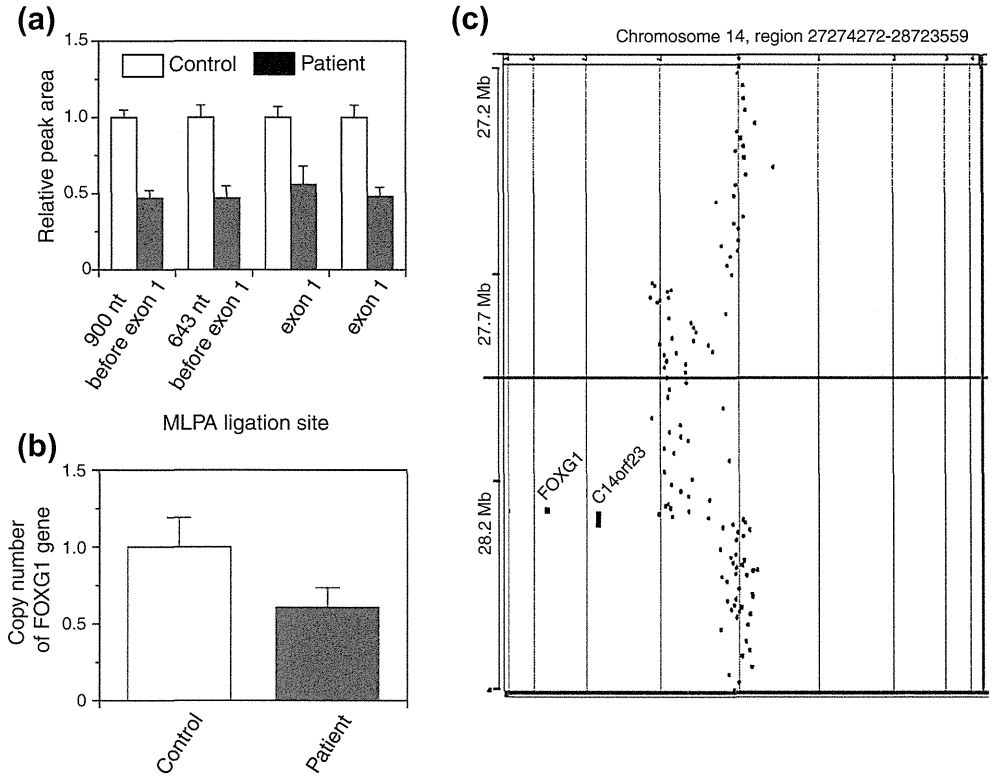

Fig. 2. Heterozygous deletion of the *FOXG1* in the patient. (a) MLPA analysis performed on DNA from the patient revealed deletion of exon 1 in *FOXG1* and a region upstream of exon 1. Results indicate the relative peak area of a probe target sequence with normalization against normal male samples and are shown as means ± SD ($n = 4$). (b) The number of *FOXG1* copies was ascertained using quantitative real-time PCR assay based on the relative amplification of the target sequence (*FOXG1*) and the internal standard *RNaseP*. Results show the ratio of *FOXG1* versus *RNaseP* gene copies, shown as means ± SD ($n = 4$). (c) The array-CGH result shows the log2 intensity ratios of the patient versus reference DNA. A 0.54-Mb deletion was detected at 14q12. This region includes only two genes: *FOXG1* and *C14orf23*.

DNA using an MLPA kit (MLPA-P075-A1; MRC-Holland, Amsterdam, The Netherlands) revealed a deletion in 14q12 including exon 1 of *FOXG1* and a region upstream of exon 1 (Fig. 2a). Gene dosage analysis was performed using quantitative real-time PCR [4], which confirmed the deletion of *FOXG1* in the patient (Fig. 2b). Testing of the patient's parents confirmed that the deletion of *FOXG1* was *de novo*. To define the boundary of the deleted region, array-based comparative genomic hybridization (aCGH) analysis was performed using a high-resolution 400 K array (Agilent Technologies Inc., Santa Clara, CA, USA) according to the manufacturer's instructions. As a consequence, 540 Kb deletion was confirmed at 14q12 from 27.78 to 28.32 Mb (Fig. 2c; according to UCSC Human Genome Browser, on March 2006 Assembly). Only two genes are included in the region: *FOXG1* and a putative gene, *C14orf23*, with unknown function.

4. Discussion

This report described a Japanese boy with a *de novo* heterozygous deletion of *FOXG1*. *FOXG1*-related disorders consist of 14q12 microdeletion syndrome, loss of function mutation in *FOXG1* and 14q12 microduplication syndrome [4–9,14,15]. *FOXG1* is located on the autosomal chromosome. However, *FOXG1* abnormalities have been found more frequently in females than in males, probably because of the predominance of females in the diagnosis of RTT. This case report confirmed that *FOXG1* haploinsufficiency causes the congenital variant of RTT in males as well as in females.

His neurological symptoms and brain MRI findings were consistent with a diagnosis of congenital variant of RTT. Patients with 14q12 microdeletion or *FOXG1* point mutation show cardinal clinical features including severe psychomotor deterioration after 3–6 months, acquired microcephaly, truncal hypotonia, epilepsy, and involuntary movements such as tongue protrusion and stereotyped jerky movements of the upper limbs. Brain MRI findings of patients with 14q12 microdeletion or *FOXG1* point mutation are indicate hypogenesis of the rostral part of the corpus callosum and delayed myelination that is specific to frontal lobe. In 2006, Bisgaard et al. reported the first case of microdeletion in chromosome band 14q12, resulting in haploinsufficiency for *FOXG1* [4,5]. Since that first case, more than 10 such cases have been reported [6–8]. In 2008, Ariani et al. reported the first two cases with point mutations of *FOXG1* [4]. In 2009, Yeung et al. reported a case of microduplication in chromosome band 14q12 including *FOXG1* [14]. A considerable phenotypic overlap exists between patients with 14q12 microdeletion, loss of function of mutation in *FOXG1*, 14q12 microduplication, and our patient (presented in

Table 1
Summary of clinical findings of this case, 14q12 microdeletion, *FOXG1* point mutation, and 14q12 microduplication.

	This study	14q12 microdeletion [4,5]	*FOXG1* point mutation [3]	14q12 microduplication [9,10]
Psychomotor deterioration	After 3 months	After 3–6 months	After 3 months	Sometimes after 3 months
Developmental delay	Postnatal onset	Postnatal onset	Postnatal onset	From birth
Hypotonia	+	+	+	Sometimes
Microcephaly	Postnatal onset	Postnatal onset	Postnatal onset or congenital	Sometimes postnatal
Epilepsy	Refractory	Treatable	Treatable	Sometimes refractory infantile spasms
Involuntary movements				
Jerky movements	+	+	+	–
Tongue protrusion	+	+	+	–
Hand stereotypies	–	+	+	–
Sleep disturbance	+	Sometimes	Sometimes	–
Feeding problems	–	+	Sometimes	–
Brain MRI				
Corpus callosum	Hypogenesis	Sometimes agenesis	Hypogenesis	Hypogenesis
White matter	Delayed myelination (frontal lobe)	Delayed myelination	Delayed myelination	Reduction of white matter volume
Cortex	No abnormality	Not reported	Gyral simplification (frontal lobe)	Not reported
Dysmorphisms	Round face Anteverted nostril Tented upper lips	Epicanthic folds Bulbous nasal tip Depressed nasal bridge Tented upper lips	Not significant	Mid face hypoplasia Flat nasal bridge Small palpebral fissures

the Table 1), suggesting a dosage-sensitive role for *FOXG1* in brain development [14]. FOXG1 plays an important role in forebrain development [10–12]. These developmental abnormalities, which were specific to the forebrain, appear to be a key feature associated with *FOXG1* haploinsufficiency, although patients with 14q12 microduplication showed no specific abnormalities of the brain MRI [14,15].

Facial dysmorphisms including epicanthic folds, bulbous nasal tip, depressed nasal bridge, and tented upper lips have often been demonstrated in patients with 14q12 microdeletions. By contrast, these features are not seen in patients with *FOXG1* point mutations. It seems likely that the facial dysmorphisms are caused by a contiguous deletion of other genes at 14q12. However, our patient and a previously reported patient [16] who have deletions of only two genes, *FOXG1* and a putative gene *C23orf14C14orf23*, also show distinctive facial features similar to patients with 14q12 microdeletions. Because the identified deletion was the smallest among those previously reported, this deletion narrowed the critical region for facial dismorphism. Consequently, *C14orf23* might be responsible for facial dysmorphism. Further investigations must be conducted to elucidate the function of *C14orf23* for facial dysmorphism.

Acknowledgment

We thank the members of the patient's family, whose help and participation made this work possible.

References

[1] Amir RE, Van den Veyver IB, Wan M, Tran CQ, Francke U, Zoghbi HY. Rett syndrome is caused by mutations in X-linked *MECP2*, encoding methyl-CpG-binding protein2. Nat Genet 1999;23:185–8.

[2] Scala E, Ariani F, Mari F, Caselli R, Pescucci C, Longo I, et al. CDKL5/STK9 is mutated in Rett syndrome variant with infantile spasms. J Med Genet 2005;42:103–7.

[3] Liang JS, Shimojima K, Takayama R, Natsume J, Shichiji M, Hirasawa K, et al. *CDKL5* alterations lead to early epileptic encephalopathy in both genders. Epilepsia 2011;52:1835–42.

[4] Ariani F, Hayek G, Rondinella D, Artuso MA, Spanhol-Rosseto A, Pollazzon M, et al. *FOXG1* is responsible for the congenital variant of Rett syndrome. Am J Hum Genet 2008;83:89–93.

[5] Bisgaard AM, Kirchhoff M, Tumer Z, Jepsen B, Brondum-Nielsen K, Cohen M, et al. Additional chromosomal abnormalities in patients with previously detected abnormal karyotype, mental retardation, and dysmorphic features. Am J Med Genet A 2006;140:2180–7.

[6] Papa FT, Mencarelli MA, Caselli R, Katzaki E, Sampieri K, Melini I, et al. A 3 Mb deletion in 14q12 causes severe mental retardation, mild facial dysmorphisms and Rett-like features. Am J Med Genet A 2008;146A:1994–8.

[7] Mencarelli MA, Kleefstra T, Katzaki E, Papa FT, Cohen M, Pfundt R, et al. 14q12 microdeletion syndrome and congenital variant Rett syndrome. Eur J Med Genet 2009;52:148–52.

[8] Florian C, Bahi-Buisson N, Bienvenn T. *FOXG1*-related disorders: from clinical description to molecular genetics. Mol Syndromol 2011;2:153–63.

[9] Pintandi M, Calevo MG, Vignoli A, Parodi E, Ajello F, Baglietto MG. Epilepsy in Rett syndrome: clinical and genetic features. Epilepsy Behav 2010;19:296–300.

[10] Hanashima C, Li SC, Shen L, Lai E, Fishell G. Foxg1 suppresses early cortical cell fate. Science 2004;303:56–9.

[11] Danesin C, Houart C. Developmental mechanisms, patterning and evolution A Fox stops the Wnt: implications for forebrain development and diseases. Curr Opin Genet Dev 2012;4:323–30.

[12] Filippis RD, Pancrazi L, Bjogo K, Rosset A, Kleefstra T, Grillo E, et al. Expanding the phenotype associated with *FOXG1* mutations and in vivo FoxG1 chromatin-binding dynamics. Clin Genet 2012;4:395–403.

[13] Neul JL, Kaufmann WE, Glaze DG, Christodoulou J, Clarke AJ, Bahi-Buisson N, et al. Rett search consortium. Rett syndrome: revised diagnostic criteria and nomenclature. Ann Neurol 2010;68:944–50.

[14] Yeung A, Bruno D, Scheffer IE, Carranza D, Burgess T, Slater HR, et al. 4.45 Mb microduplication in chromosome band 14q12 including *FOXG1* in a girl with refractory epilepsy and intellectual impairment. Eur J Med Genet 2009;52:440–2.

[15] Brunetti-Pierri N, Paciokowski AR, Ciccone R, Della Mina E, Bonaqlia MC, Borqatti R, et al. Duplications of *FOXG1* in 14q12 are associated with developmental epilepsy, mental retardation, and severe speech impairment. Eur J Hum Genet 2011;19:102–7.

[16] Jacob FD, Ramaswamy V, Andersen J, Bolduc FV. Atypical Rett syndrome with selective *FOXG1* deletion detected by comparative genomic hybridization: case report and review of literature. Eur J Hum Genet 2009;17:1577–81.

Journal of Neurochemistry JNC

JOURNAL OF NEUROCHEMISTRY | 2014 | 128 | 280–293 doi: 10.1111/jnc.12505

ORIGINAL ARTICLE

Identification of two novel *Shank3* transcripts in the developing mouse neocortex

Chikako Waga,*,† Hirotsugu Asano,* Tomomi Sanagi,* Eri Suzuki,* Yasuko Nakamura,* Akiko Tsuchiya,* Masayuki Itoh,† Yu-ichi Goto,† Shinichi Kohsaka* and Shigeo Uchino*,‡

*Department of Neurochemistry, National Institute of Neuroscience, Kodaira, Tokyo, Japan

†Department of Mental Retardation and Birth Defect Research, National Institute of Neuroscience, Kodaira, Tokyo, Japan

‡Department of Biosciences, School of Science and Engineering, Teikyo University, Utsunomiya, Tochigi, Japan

Abstract

SHANK3 is a synaptic scaffolding protein enriched in the post-synaptic density of excitatory synapses. Since several SHANK*3* mutations have been identified in a particular phenotypic group of patients with autism spectrum disorder (ASD), SHANK3 is strongly suspected of being involved in the pathogenesis and neuropathology of ASD. Several SHANK3 isoforms are known to be produced in the developing brain, but they have not been fully investigated. Here, we identified two different amino-terminus truncated *Shank3* transcripts. One transcript, designated as *Shank3c-3*, produces an isoform that contains the entire carboxyl-terminus, but the other transcript, designated as *Shank3c-4*, produces a carboxyl-terminus truncated isoform. During development, expression of the novel *Shank3* transcripts increased after birth, transiently decreased at P14 and then gradually increased again thereafter. We also determined that methyl CpG-binding protein 2 (MeCP2) is involved in regulating expression of the novel *Shank3* transcripts. MeCP2 is a transcriptional regulator that has been identified as the causative molecule of Rett syndrome, a neurodevelopmental disorder that includes autistic behavior. We demonstrated a difference between the expression of the novel *Shank3* transcripts in wild-type mice and *Mecp2*-deficient mice. These findings suggest that the SHANK3 isoforms may be implicated in the synaptic abnormality in Rett syndrome.

Keywords: autism spectrum disorder, DNA methylation, MeCP2, SHANK3.

J. Neurochem. (2014) **128**, 280–293.

The *SHANK3/proline-rich synapse-associated protein 2 (PROSAP2)* gene consists of 22 exons and encodes a multidomain protein that contains ankyrin repeats (ANK) in an amino-terminal region, an Src homology 3 domain, a post-synaptic density 95/discs large/zone occludens-1 domain, a proline-rich region, a homer-binding region, a cortactin-binding region and a sterile alpha motif (SAM) (Naisbitt *et al.* 1999). SHANK3 is abundantly expressed in the heart and moderately expressed in the brain and spleen, and its tissue-specific expression is epigenetically regulated by DNA methylation (Lim *et al.* 1999; Beri *et al.* 2007). In the brain, SHANK3 is mainly expressed in neurons, especially in their synapses, and acts as a scaffolding protein in its interactions with various synaptic molecules, including with the NMDA receptor via the post-synaptic density-95 (PSD-95)/guanylate kinase-associated protein complex, with the metabotropic glutamate receptor via homer, and with the GluR1 alpha-amino-3-hydroxy-5-methylisoxazole-4-propionate receptor (Lim *et al.* 1999; Naisbitt *et al.* 1999; Sheng and Kim 2000; Boeckers *et al.* 2004; Uchino *et al.* 2006).

Received May 14, 2013; revised manuscript received October 2, 2013; accepted October 18, 2013.

Address correspondence and reprint requests to Shigeo Uchino, Department of Biosciences, School of Science and Engineering, Teikyo University, 1-1 Toyosatodai, Utsunomiya, Tochigi 320-8551, Japan. E-mail: uchino@nasu.bio.teikyo-u.ac.jp

Abbreviations used: AMPA, alpha-amino-3-hydroxy-5-methylisoxazole-4-propionate; ASD, autism spectrum disorder; MeCP2, methyl CpG-binding protein 2; SH3, Src homology 3; PDZ, post-synaptic density 95/discs large/zone occludens-1; SAM, sterile alpha motif.

Haploinsufficiency of the *SHANK3* gene causes a developmental disorder, 22q13.3 deletion syndrome, also known as Phelan-McDermid syndrome, which is characterized by severe expressive language and speech delay, hypotonia, global developmental delay, and autistic behavior (Bonaglia *et al.* 2001). Since numerous abnormalities in the *SHANK3* gene have been identified in a particular phenotypic group of patients with autism spectrum disorder (ASD), SHANK3 is strongly suspected of being involved in the pathogenesis and neuropathology of ASD (Durand *et al.* 2007; Moessner *et al.* 2007; Gauthier *et al.* 2009; Waga *et al.* 2011).

Several lines of *Shank3*-mutant mice have been generated and used to investigate the contribution of SHANK3 to the neuropathology of ASD (Bozdagi *et al.* 2010; Peça *et al.* 2011; Wang *et al.* 2011; Schmeisser *et al.* 2012; Yang *et al.* 2012; Jiang and Ehlers 2013). Mice that lack the full length of SHANK3 have been found to exhibit synaptic dysfunction and abnormal synaptic morphology and to display ASD-relevant phenotypes, including abnormal social behaviors, abnormal communication patterns, repetitive behaviors, and deficits in learning and memory, but several different SHANK3 isoforms were still expressed in the mutant mice. Peça and coworkers recently generated two *Shank3*-deficient mouse strains: a *Shank3A* mutant strain (*Shank3A*$^{-/-}$) lacking exons 4–7 and a *Shank3B* mutant strain (*Shank3B*$^{-/-}$) lacking exons 13–16 (Peça *et al.* 2011). The full length of SHANK3 (SHANK3α) is disrupted in *Shank3A*$^{-/-}$ mice but other isoforms are unaffected, whereas an amino-terminus truncated SHANK3 isoform lacking ANK (SHANK3β) as well as SHANK3α is absent in *Shank3B*$^{-/-}$ mice. Interestingly, a three-chamber social test demonstrated that the *Shank3B*$^{-/-}$ mice exhibited abnormal social interaction and discrimination of social novelty, whereas the *Shank3A*$^{-/-}$ mice, in which only SHANK3α is absent, displayed normal initiation of social interaction, but impaired recognition of social novelty. The *Shank3B*$^{-/-}$ mice displayed an anxiety-like behavior and excessive, self-injurious grooming, whereas the *Shank3A*$^{-/-}$ mice did not display any anxiety-like behavior and lesions. These findings suggest that dysfunction of the SHANK3 isoform is probably involved in the phenotypic heterogeneity in ASD.

Several SHANK3 isoforms are known to be produced in the mouse brain by combinations of multiple intragenic promoters and alternative splicing processes (Wang *et al.* 2011; Jiang and Ehlers 2013). The *SHANK3* gene contains five CpG islands (CpG-P and CpG-2 - CpG-5), and the positions of five CpG islands are well conserved in mammalian (Ching *et al.* 2005; Beri *et al.* 2007). Maunakea *et al.* recently demonstrated that some intragenic promoters are regulated by DNA methylation in CpG islands (Maunakea *et al.* 2010). However, the methylation status of the CpG islands in the *SHANK3* gene in the developing brain has not been fully investigated. In this study, we demonstrated differences between the methylation status of the five CpG islands in the developing mouse brain and identified novel SHANK3 transcripts whose transcriptional start sites are located in intron 10 in the vicinity of CpG island-2.

Materials and methods

Sequence of mouse *Shank3* gene

The genome sequence of the *Shank3* gene is available at the NCBI database (NC_000081.6), and the cDNA sequence is available at the GenBank database (AB231013).

Animals

The animals used in this study were Crl:CD-1 (ICR) mice (CLEA Japan, Tokyo, Japan), heterozygous *Mecp2*-deficient female mice (B6.129P2 (C)-*Mecp2* $^{tm1.1\ Bird/J}$; Jackson Laboratory, Maine, USA) (Guy *et al.* 2001) and C57BL/6JJcl male mice (CLEA Japan), which were used for mating with *Mecp2*-deficient female mice. All experimental procedures were approved by The Animal Care and Use Committee of the National Institute of Neuroscience.

Analysis of the methylation status of the CpG islands

Genomic DNA was extracted from mouse neocortical tissue (gray matter) at embryonic day 17 (E17), post-natal day 1 (P1), P7, P14, P21, P28, and 12 weeks after birth (12W) using the Wizard Genomic DNA Purification Kit (Promega, Madison, WI, USA). Three mice were used at each developmental stage. Methylation status was determined by the *Hpa*II-*Mcr*BC PCR method using two restriction enzymes having complementary methylation sensitivity, *Hpa*II and *Mcr*BC, as described in a previous study (Yamada *et al.* 2004). PCR was performed by using PrimeSTAR DNA polymerase (Takara, Shiga, Japan) and a thermal cycler (GeneAmp PCR System 9700; Life Technologies, Grand Island, NY, USA). The primer sequences, annealing temperatures, cycles, and sizes of the PCR products are shown in Table S1. The following primer pairs were used: CpGP-F/CpGP-R for CpG island-P, In10-F/CpG2-R for CpG island-2, CpG3-F/CpG3-R for CpG island-3, CpG4-F/CpG4-R for CpG island-4, CpG5-F/CpG5-R for CpG island-5, and 5UTR-F/5UTR-R as a control. The thermocycling conditions were: 60 s at 98°C, 30 s at the annealing temperature, 60 s at 72°C for 33–45 cycles. The PCR products were electrophoretically separated on an agarose gel and stained with ethidium bromide. The gel images were fed into an image analyzer (LAS-3000 mini; FUJIFILM, Tokyo, Japan) and quantitatively analyzed with ImageJ software (National Institutes of Health, Bethesda, MD, USA). The data were obtained from three independent PCR experiments.

Total RNA preparation, cDNA synthesis, and real-time PCR

Total RNA was extracted from mouse neocortical tissue (gray matter) with acid guanidinium thiocyanate–phenol–chloroform at E17, P1, P7, P14, P21, P28, and 12W (Chomczynski and Sacchi 1987), and cDNA was produced by using the Advantage RT for PCR kit (Clontech, Palo Alto, CA, USA) according to the manufacturer's instructions. Three mice were used at each developmental stage.

PCR for analysis of expression of the novel *Shank3* transcripts was performed using PrimeSTAR DNA polymerase with GC buffer (Takara) and a thermal cycler (GeneAmp PCR System 9700). The thermocycling conditions were: 60 s at 98°C, 30 s at 60°C, 60 s at 72°C for 40 cycles for brain tissue and 45 cycles for Neuro2A cells. The primers used were In10-F and Ex14-R, and their sequences are listed in Table S2.

Real-time PCR was performed by using the SYBR green labeling system (Power SYBR Green PCR Master Mix; Life Technologies) and the ABI Prism 7700 Sequence Detection System (Life Technologies). The primer sequences and sizes of the PCR products are shown in Table S2. Amplifications were carried out in a 384-well optical plate, and the thermocycling conditions were: 5 s at 95°C, 10 s at 60°C, and 30 s at 72°C for 45 cycles. A quantitative analysis was performed by the delta-delta Ct method with glyceraldehyde-3-phosphate dehydrogenase used as an internal control (Ermolinsky *et al.* 2008). The data were obtained from four independent PCR experiments.

5′-Rapid Amplification of cDNA Ends (5′-RACE)

Total RNA was prepared from the neocortical tissue (gray matter) of P14 mice, and 5′-RACE was performed by using the GeneRacer kit (Life Technologies) according to the manufacturer's instructions. PCR was performed by using AmpliTaq Gold 360 Master Mix (Life Technologies) and a thermal cycler (GeneAmp PCR System 9700). The initial thermocycling conditions were as follows: 30 s at 98°C and 60 s at 72°C for 5 cycles, 30 s at 98°C and 60 s at 70°C for 5 cycles, and then 30 s at 98°C, 30 s at 65°C, 60 s at 72°C for 30 cycles, and the primers used were GeneRacer 5′-primer (5′-CGACTGGAGCACGAGGACACTGA-3′) and Ex14-R2 primer (5′-GGATAGCCACCTTATCATCGATGACATAATCG-3′). The second thermocycling conditions were: 30 s at 98°C, 30 s at 65°C, 60 s at 72°C for 30 cycles, and the primers used were the GeneRacer 5′-Nested primer (5′-GGACACTGACATGGACT GAAGGAGTA-3′) and Ex14-R2 primer. The PCR product was subcloned into pGEM-T Easy vector (Promega) by the TA cloning method, and the DNA sequence was determined by using an ABI3100-*Avant* genetic analyzer (Life Technologies).

Identification of *Shank3* transcripts

The full length of the *Shank3* transcript expressed from the intron 10 region was cloned by the RT-PCR method. The cDNA produced from neocortical total RNA at P14 was used as a template DNA. PCR was performed using KOD-plus- (TOYOBO, Tokyo Japan) and a thermal cycler (GeneAmp PCR System 9700). The thermocycling conditions were: 10 s at 98°C and 8 min at 68°C for 5 cycles, and then 10 s at 98°C, 30 s at 62°C, 8 min at 68°C for 30 cycles, and the primers used were In10-F and 3UTR-R (5′-AGGG CCCCCCACCCCACAGGTCATT-3′). The PCR products were subcloned into pGEM-T Easy vector (Promega) by the TA cloning method, and at least two different *Shank3* constructs were obtained: pGEM-Shank3c-3, which contained part of the sequence coded by intron 10 and a completely spliced form from exon 11 to exon 22, and pGEM-Shank3c-4, which lacked the sequences coded by exon 21. The DNA sequences were determined with an ABI3100-*Avant* genetic analyzer.

Plasmid construction

The construction of the plasmids used in this study is described in detail in the experimental procedure and Figure S1 and Figure S2 in the supplemental information.

Cell culture and DNA transfection

Neuro2A cells and HEK293 cells were grown at 37°C in Dulbecco's modified Eagle's medium (Life Technologies) containing 10% heat-inactivated fetal bovine serum under a humidified 5% CO_2 atmosphere. Neuro2A cells were plated at a density of 1.0–3.0 $\times$ 10^4 cells/cm^2 and maintained for 2 days in medium containing a 1 μM or 5 μM concentration of 5-Aza-2′-deoxycytidine (5-AdC; Wako, Osaka, Japan). For the luciferase assays, HEK293 cells were plated in each well of 12-well culture dishes at a density of 5.0 $\times$ 10^4 cells/well, maintained for 2 days, and then transfected with a plasmid DNA by using TransIT-LT1 (Mirus Bio, Madison, WI, USA) according to the manufacturer's instructions. After 2 days, the cells were harvested and used for the luciferase assay. For immunoblot analysis, HEK293 cells were plated at a density of 1.0 $\times$ 10^4 cells/cm^2, maintained for 2 days, and then transfected with a plasmid DNA by using Lipofectamine Plus (Life Technologies) according to the manufacturer's instructions. After 2 days, the cells were harvested and used for the immunoblot analysis.

Embryonic day 15.5 ICR mouse neocortical primary neurons were prepared as described previously (Hirasawa *et al.* 2003). Briefly, cerebral cortices were dissected, minced and dissociated with papain. The dissociated cells were plated onto 0.1% polyethyleneimine-coated plates at a density of 1.5–3.0 $\times$ 10^4 cells/cm^2 for immunocytochemistry and at a density of 5.0 $\times$ 10^4 cells/cm^2 for luciferase assays, and maintained in Neurobasal (NB) medium (Life Technologies) containing 2% B-27 supplement (Life Technologies) and 0.5 mM glutamine (NB-s-medium) at 37°C under a humidified 10% CO_2 atmosphere for the indicated periods. For the transient expression studies, cells were transfected with a plasmid DNA by using Lipofectamine 2000 (LF2000; Life Technologies) according to the manufacturer's instructions, with slight modifications. Plasmid DNA that had been diluted with NB medium and LF2000 Reagent that had been diluted with NB medium were combined and incubated for 15–20 min at 20–25°C. The DNA-LF2000 Reagent complex was added to the cells, and they were maintained at 37°C in a 10% CO_2 incubator for 1–2 h. After washing with fresh NB medium the cells were maintained in conditioned medium that consisted of equal volumes of fresh NB medium and spent medium harvested from cultured cells. Half of the medium was replaced with fresh NB-s-medium every 3–4 days.

Luciferase assay

Luciferases assays were performed by using the Dual-Luciferase Reporter Assay System (Promega) according to the manufacturer's instructions, and reporter activity was measured with a Centro LB960 plate reader (Berthold Technologies, Bad Wildbad, Germany). The firefly luciferase value of each sample was divided by the renilla luciferase value to average the independent transfection. Each plasmid was transfected into cells cultured in three separate wells, and three independent transfections were performed.

Immunocytochemistry

Cells were fixed with 2% paraformaldehyde for 10 min at 20–25°C. After three washes with phosphate-buffered saline (PBS) at 5-min intervals, the cells were permeabilized and blocked in PBS containing 3% normal goat serum and 0.1% Triton X-100 for 15 min, and then incubated for 1 h at 20–25°C with the following primary antibodies in PBS containing 3% bovine serum albumin : rabbit polyclonal anti-enhanced green fluorescent protein (EGFP) antibody (1 : 500, Life Technologies), mouse monoclonal anti-MAP-2 antibody (1 : 500, Sigma, St Louis, MO, USA), rabbit polyclonal anti-Shank3 antibody (1 : 1000) (Uchino *et al.* 2006), or mouse monoclonal anti-myc antibody (clone 9E10) (1 : 300, Thermo Scientific, Rockford, IL, USA). After washing three times with PBS at 5-min intervals, the cells were incubated for 1 h at 20–25°C with the secondary antibodies in PBS containing 3% bovine serum albumin: Alexa Fluor 488 goat anti-rabbit IgG (H+L) (1 : 1000, Life Technologies), Alexa Fluor 488 goat anti-mouse IgG (H+L) (1 : 1000, Life Technologies), Alexa Fluor 594 goat anti-rabbit IgG (H+L) (1 : 1000, Life Technologies), or Alexa Fluor 594 goat anti-mouse IgG (H+L) (1 : 1000, Life Technologies). After washing three times with PBS at 5-min intervals, the cells were mounted on a glass slide with Fluoromount-G (Southern Biotech, Birmingham, AL, USA). Fluorescence images were obtained with a fluorescence microscope (AX70; Olympus, Tokyo, Japan) or a confocal laser microscope (FV1000; Olympus).

Preparation of protein samples and immunoblot analysis

HEK293 cells or neocortex tissue were homogenized and sonicated in lysis buffer (10 mM Tris-HCl (pH 7.4), 150 mM NaCl, 1 mM EDTA, 1% Triton X-100, 0.1% sodium dodecyl sulfate and a protease inhibitor cocktail (Roche, Penzberg, Germany). After removing the nuclei and debris by centrifugation (2000 x *g* for 10 min at 4°C), the protein concentration of the supernatant was determined using BCA Protein Assay Kit (Pierce, Rockford, IL, USA), and the supernatant was stored at −80°C until used.

The protein samples were separated by electrophoresis through an sodium dodecyl sulfate polyacrylamide gel: a 5% gel for neocortical samples and a 5–20% gradient gel (Dream Realization & Communication (DRC), Tokyo, Japan) for HEK293 cells, and then electrophoretically transferred to nitrocellulose membranes (Schleicher & Schuell, Dassel, Germany). The membranes were blocked overnight with 3% skim milk in Tris-buffered saline containing 0.1% Tween20 (TBS-T) at 4°C, then incubated at 20–25°C for 3 h in 3% skim milk in TBS-T containing rabbit polyclonal anti-Shank3 antibody (1 : 3000) (Uchino *et al.* 2006), mouse monoclonal anti-myc antibody (clone 9E10) (1 : 1500), or mouse monoclonal anti-β actin antibody (1 : 1500; Sigma). After three washes in TBS-T, the membranes were incubated at 20–25°C for 1 h with horseradish peroxidase-conjugated anti-rabbit IgG secondary antibody (1 : 1500; Sigma) or horseradish peroxidase-conjugated anti-mouse IgG secondary antibody (1 : 1500; GE Healthcare, Buckinghamshire, UK), and washed three times with TBS-T. Immunoreactive bands were visualized with a chemiluminescence detection system (ECL; GE Healthcare) and the images were fed into an image analyzer (LAS-3000 mini).

Chromatin immunoprecipitation (ChIP)

Fresh mouse neocortical tissue (gray matter, 100–150 mg) was dissected out, chopped into small pieces, and homogenized. ChIP was performed by using the ChIP assay kit (Millipore, Temecula, CA, USA) and rabbit polyclonal anti-Mecp2 antibody (Millipore) according to their manufacturers' instructions. PCR was performed by using GoTaq DNA polymerase (Promega) and a thermal cycler (GeneAmp PCR System 9700). The primer sequences, annealing temperatures, and sizes of the PCR products are shown in Table S1. The primer pairs used were: In10-F/CpG2-R for CpG island-2, CpG3-F/CpG3-R for CpG island-3, CpG4-F/CpG4-R for CpG island-4, and CpG5-F/CpG5-R and CpG5-F2/CpG5-R for CpG island-5. The thermocycling conditions were as follows: 30 s at 98°C, 30 s at annealing temperatures, 60 s at 72°C for 45 cycles. The PCR with the In10-F and CpG2-R primer pair was performed under 5% dimethyl sulfoxide.

Statistical analysis

All values were expressed as the mean ± SEM of n independent observations. Multiple groups were compared by one-way analysis of variance (ANOVA), which was followed by Dunnett's test when two groups were compared. Differences were considered significant when the p-value was < 0.05.

Results

Methylation analysis of the CpG islands in the mouse *Shank3* gene

To investigate the methylation status of the five CpG islands (CpG-P and CpG-2 - CpG-5 shown in Fig. 1a) in the developing mouse brain, genomic DNA was extracted from mouse neocortical tissue at E17, P1, P7, P14, P21, P28, and 12 weeks after birth (12W), and the methylation status of the CpG islands was assessed by the *Hpa*II-*Mcr*BC PCR method (Yamada *et al.* 2004). *Hpa*II digests unmethylated alleles at CCGG sites, and *Mcr*BC digests methylated alleles at $Pu^mC(N_{40-2000})Pu^mC$, When a sequence is fully methylated, *Hpa*II fails to digest the target site, whereas *Mcr*BC digests it completely. Therefore, a PCR product of a target region is detected only from the *Hpa*II-digested template. Since PCR products at CpG island-P were detected only from the *Mcr*BC-digested template (lane U in Fig. 1b) and PCR products at CpG island-3 were detected only from the *Hpa*II-digested template (lane M in Fig. 1b), the results showed that CpG island-P was completely unmethylated and CpG island-3 was fully methylated at every stage of development investigated, whereas the methylation rate of CpG island-2, -4, and -5 were low in the embryonic stage, but significantly increased after birth. Interestingly, the methylation rate of CpG island-2 increased until P14 and gradually decreased thereafter (Fig. 1b and c).

A novel *Shank3* transcript in intron 10

Since Beri and coworkers reported finding dramatic differences in the methylation status of CpG island-2 in various

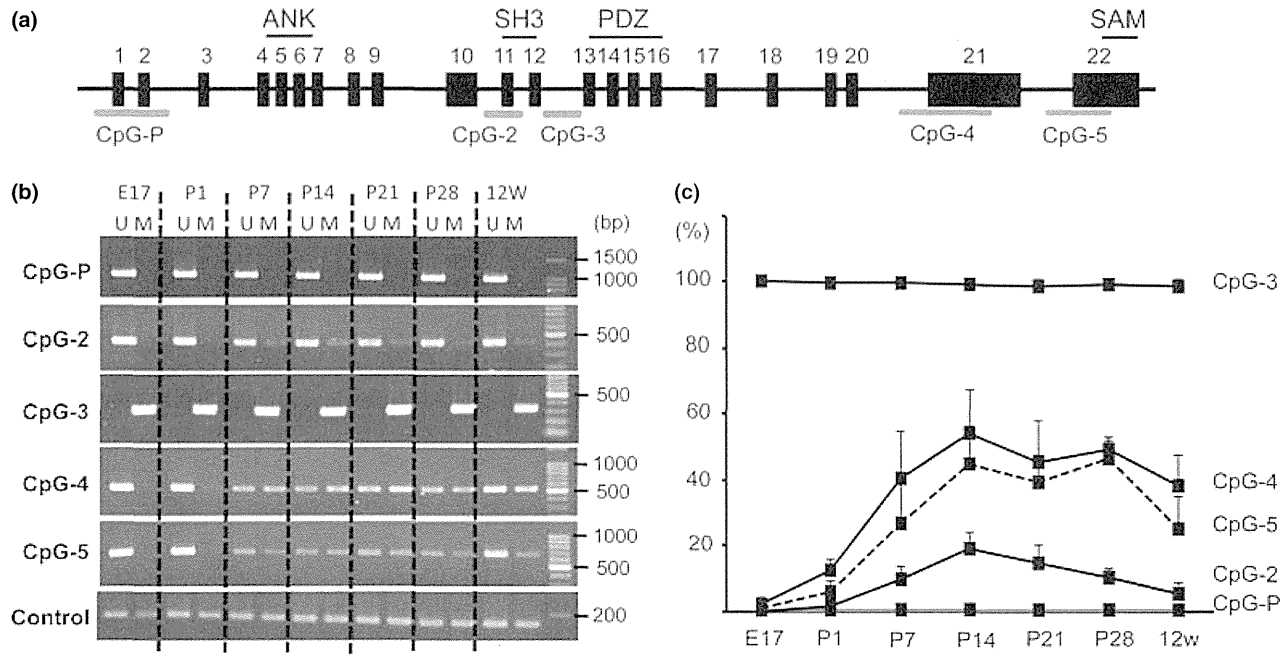

Fig. 1 Methylation status of the intragenic CpG-islands of the *Shank3* gene in the developing mouse neocortex. (a) Schematic structure of the mouse *Shank3* gene. Exons (1–22) are represented by a black box, and the CpG islands identified by using a Methyl Primer Express software (Life Technologies) are represented by a gray line. (b) Representative agarose gel electrophoresis images showing a *Hpa*II-*Mcr*BC PCR assay of the five CpG islands in the *Shank3* gene. A *Hpa*II-digested template (M) and an *Mcr*BC-digested template (U) were used. Size markers (100 bp ladder) are shown at the right. (c) Quantitative analysis of methylation status determined by a *Hpa*II-*Mcr*BC PCR assay. $n = 3$.

tissues and cell lines (Beri *et al.* 2007), we focused on CpG island-2. Because genome sequence analysis revealed high homology (94%) between an approximately 380 bp length of DNA containing CpG island-2 located upstream of exon 11 in the human gene and the mouse gene (Fig. 2a), we hypothesized expression of a novel transcript in this intragenic region. To test our hypothesis we performed RT-PCR using a forward primer within intron 10 (In10-F) and a reverse primer within exon 14 (Ex14-R), and an approximately 450 bp PCR product was detected as a result. Sequence analysis revealed that the PCR product contained part of intron 10 and a completely spliced form from exon 11 to exon 14 of the *Shank3* gene (Fig. 2b). Expression of this transcript was weak at E17 but increased after birth. Interestingly, its expression transiently decreased at P14, when the methylation rate in CpG island-2 was the highest, but increased thereafter (Fig 2c). We quantified its expression level in the developing mouse brain by a real-time PCR (Fig. 2d). To determine whether expression of the novel transcript is regulated by DNA methylation, we examined its expression in Neuro2A cells cultured for 2 days in the presence or absence of the DNA methylation inhibitor 5-AdC. As shown in Figure 2e, exposure to 5-AdC resulted in an increase in expression of the novel transcript in comparison with the control Neuro2A cells, suggesting that expression of the novel transcript is regulated by DNA methylation.

Identification of the entire sequence of the novel *Shank3* transcript in intron 10

To identify the transcriptional initiation site of the novel *Shank3* transcript, we performed a 5′-RACE-PCR, and as shown in Fig. 3, the results revealed a transcriptional initiation site (−265) in intron 10. Sequence analysis revealed two putative sites of the translational start codon (ATG): one in intron 10 and the other in exon 12 (Fig. 3a). Since Maunakea and coworkers recently found promoter activity that is regulated by intragenic DNA methylation in the upstream of CpG island-2 in intron 10 (ECR22-promoter shown in Fig. 2a), and showed that the ECR22-promoter regulates expression of the 22t *Shank3* transcript (shown in Fig. 3b) (Maunakea *et al.* 2010), we next attempted to confirm the promoter activity of the intron 10 by using a luciferase assay system. We constructed a reporter vector carrying a 297 bp or a 610 bp length of the intragenic gene containing the ECR22-promoter region (pGL3-ECR22-pro and pGL3-In10-pro, respectively, shown in Fig. 4a), and transfected it into HEK293 cells. Measurement of the luciferase activity 2 days later confirmed the presence of promoter activity in the ECR22-promoter regions

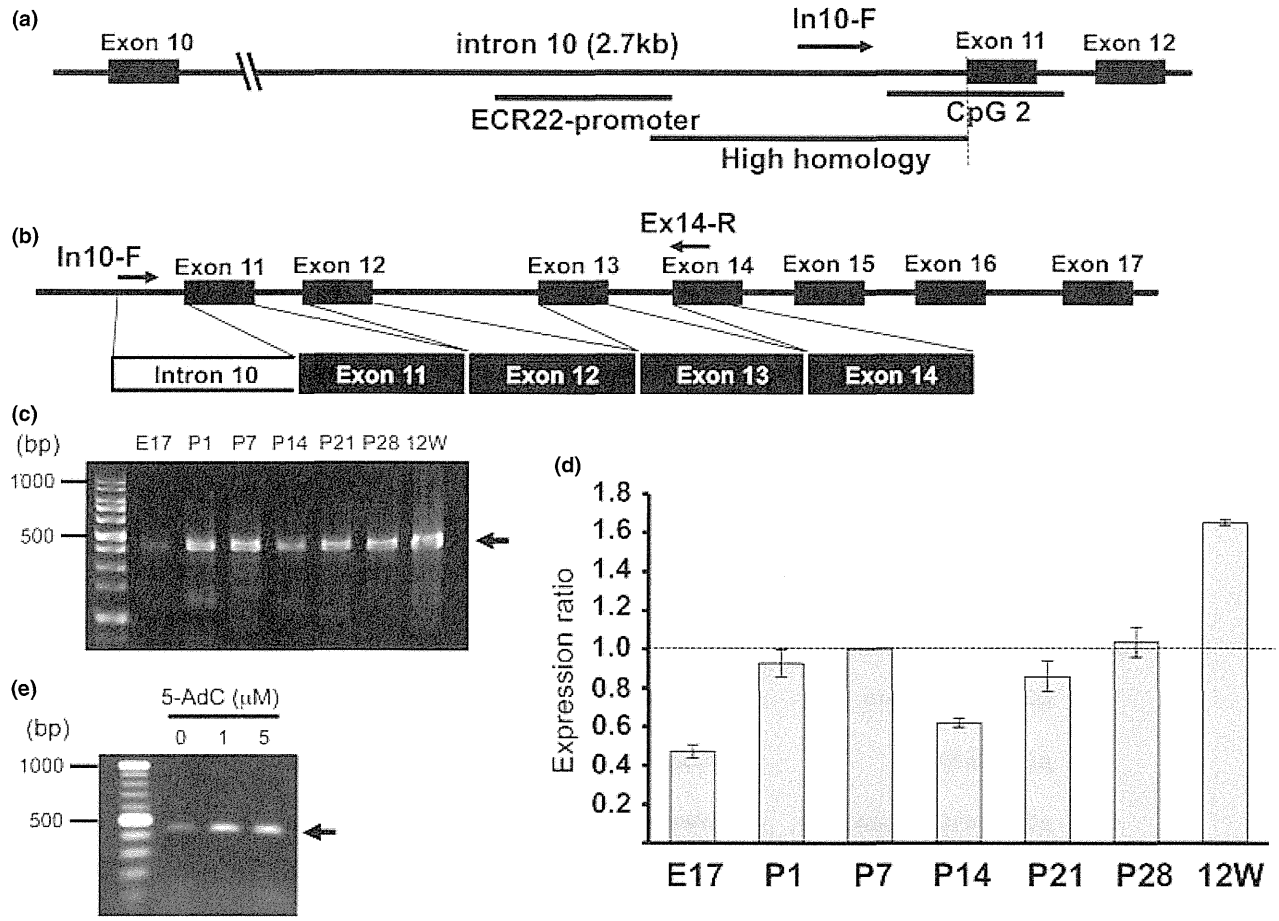

Fig. 2 Gene structure and expression profile of the novel *Shank3* transcript in intron 10. (a) Schematic structure of the mouse *Shank3* gene. Exons (10–12) are represented by a black box, and CpG island-2, a higher homology region between humans and the mouse, and the ECR22-promoter region (Maunakea *et al.* 2010) are each represented by a black line. (b) Schematic diagram of the novel *Shank3* transcript amplified by the In10-F and Ex14-R primer pair. (c) Representative agarose gel electrophoresis image showing expression of the novel *Shank3* transcript in the developing mouse neocortex after the transcript was amplified by an RT-PCR method. The arrow points to the PCR product (441 bp) amplified by the In10-F and Ex14-R primer pair. Size markers (100 bp ladder) are shown at the left. (d) Quantitative analysis of expression of the novel *Shank3* transcript by a real-time PCR using the delta-delta Ct method with glyceraldehyde-3-phosphate dehydrogenase as an internal control. The ratios were calculated by dividing the value at each stage by the value at P7. $n = 4$. (e) Representative agarose gel electrophoresis image showing expression of the novel *Shank3* transcript in Neuro2A cells in the presence of 5-AdC (1 μM, 5 μM) and in the absence of 5-AdC (0 μM). Size markers (100 bp ladder) are shown at the left.

(3.72 ± 0.12 fold), the same as found in a previous study (Maunakea *et al.* 2010), but no promoter activity was detected in the 610 bp length of the intragenic region (0.87 ± 0.06 fold) (Fig. 4b). Since sequence analysis revealed the presence of three ATG sequences within the 610 bp length of the intron region, when the ATG sequences function as a translational start codon luciferase may not be produced because of a frameshift. We then constructed two different reporter vectors, one lacking the adenine nucleotide at two positions, −293 and −186 (pGL3-In10-pro-ΔATG-2), and the other lacking the adenine nucleotide at three positions, −293, −186, and −77 (pGL3-In10-pro-ΔATG-all), in order to disrupt the ATG codon (Fig. 4a), and after transfecting each of the constructs into HEK293 cells, we measured their luciferase activity. Significant luciferase activity was observed in the cell lysate prepared from the HEK293 cells transfected with pGL3-In10-pro-ΔATG-all (2.23 ± 0.21 fold), but no luciferase activity was detected in the cell lysate prepared from the HEK293 cells transfected with pGL3-In10-pro-ΔATG-2 (0.97 ± 0.04 fold) (Fig. 4b), suggesting that the ATG sequence at position −77 functions as the translational start codon. We also confirmed the presence of luciferase activity in neocortical primary neurons transfected with pGL3-ECR22-pro (3.41 ± 0.21 fold) and pGL3-In10-pro-ΔATG-all (9.42 ± 0.67 fold) (Fig. 4c). Next, we constructed an expression vector containing an EGFP gene ligated at the ATG site at position −77 (Fig. 4a, Figure S1) and

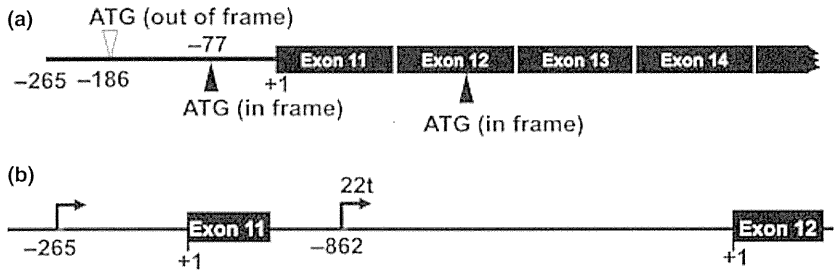

Fig. 3 Identification of the novel *Shank3* transcripts in intron 10. (a) The 5′-gene structure of the novel *Shank3* transcripts. The predicted translational start codon (ATG) is indicated by a closed arrowhead (in frame). (b) Schematic structure of the mouse *Shank3* gene. Exons 11 and 12 are represented by a black box and transcriptional initiation site of the novel *Shank3* transcript (at−265 in intron 10) and the transcriptional initiation site of 22t *Shank3* (at−862 in intron 11) (Maunakea *et al.* 2010) are each indicated by an arrow.

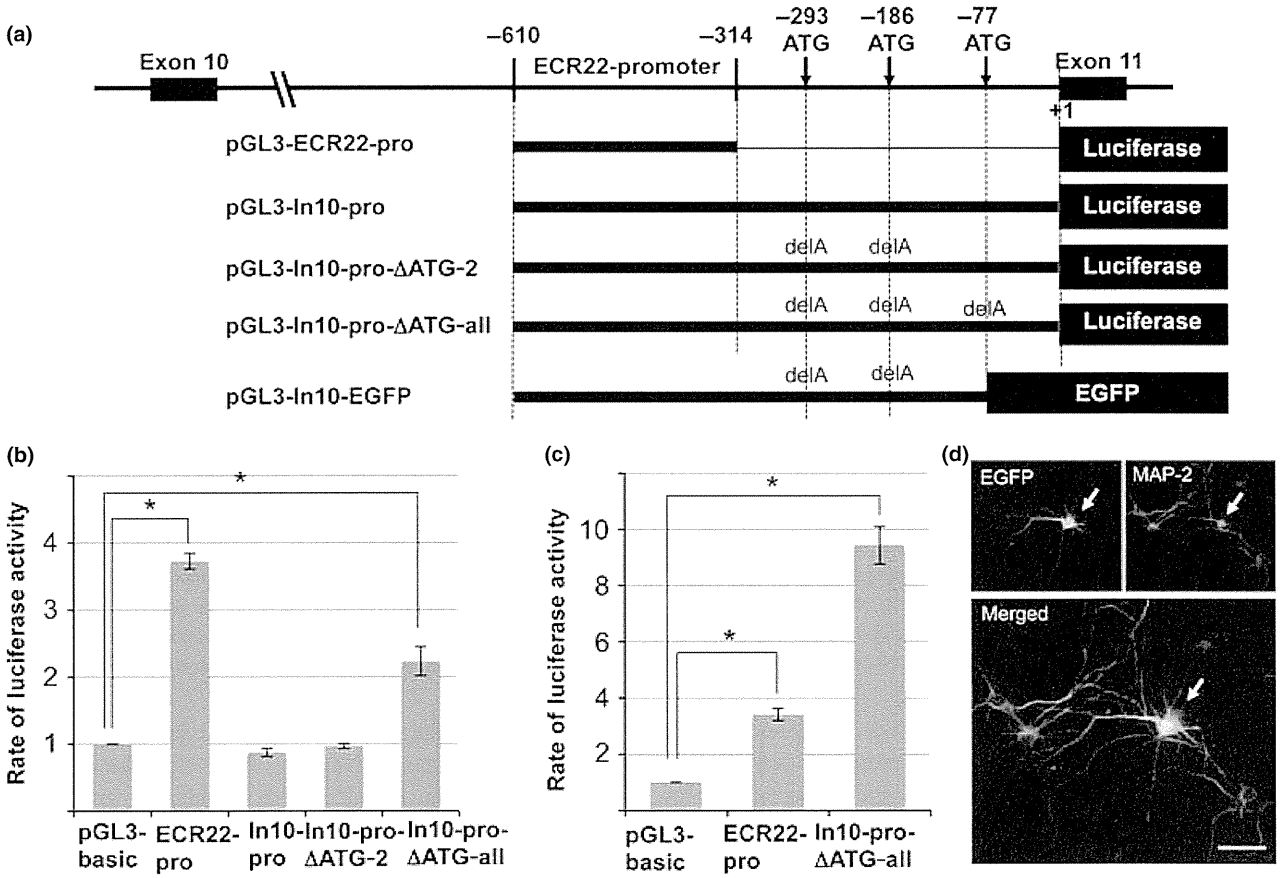

Fig. 4 Promoter activity of the DNA fragment within intron 10. (a) Schematic structure of the constructs used for the luciferase assay and enhanced green fluorescent protein (EGFP) expression. (b) Luciferase assay. HEK293 cells were transfected with the constructs, and 2 days later the cells were harvested and used for a luciferase assay. The ratios were calculated by dividing the value of each sample by the value of the control sample (pGL3-basic). *$p < 0.01$. (c) Luciferase assay. Neocortical primary neurons were cultured for 8 days and transfected with the constructs, and 2 days later the cells were harvested and used for the luciferase assay. The ratios were calculated by dividing the value of the each sample by the value of the control sample (pGL3-basic). *$p < 0.01$. (d) Representative image of immunostained neurons. Neocortical primary neurons were cultured for 8 days and transfected with pGL3-In10-EGFP, and 2 days later the cells were fixed and immunostained with anti-EGFP antibody (green) and anti-MAP-2 antibody (red). The arrow points to an EGFP- and MAP-2-positive cell. Scale bar is 20 μm.